

Article

The Role of Ovalbumin in Manganese Homeostasis during Chick Embryogenesis: An EPR Spectroscopic Study

Ana Vesković¹ , Aleksandra M. Bondžić²  and Ana Popović Bijelić^{1,*} 

¹ Faculty of Physical Chemistry, University of Belgrade, Studentski trg 12–16, 11158 Belgrade, Serbia; ana.veskovic@ffh.bg.ac.rs

² Vinča Institute of Nuclear Sciences, National Institute of the Republic of Serbia, University of Belgrade, P.O. Box 522, 11000 Belgrade, Serbia; aleksandrab@vin.bg.ac.rs

* Correspondence: ana@ffh.bg.ac.rs

Abstract: Ovalbumin (OVA), a protein vital for chick embryo nutrition, hydration, and antimicrobial protection, together with other egg-white proteins, migrates to the amniotic fluid and is orally absorbed by the embryo during embryogenesis. Recently, it has been shown that for optimal eggshell quality, the hen diet can be supplemented with manganese. Although essential for embryonic development, manganese in excess causes neurotoxicity. This study investigates whether OVA may be involved in the regulation of manganese levels. The binding of Mn(II) to OVA was investigated using electron paramagnetic resonance (EPR) spectroscopy. The results show that OVA binds a maximum of two Mn(II) ions, one with slightly weaker affinity, even in a 10-fold excess, suggesting it may have a protective role from Mn(II) overload. It seems that the binding of Mn(II), or the presence of excess Mn(II), does not affect OVA's tertiary structure, as evidenced from fluorescence and UV/vis measurements. Comparative analysis with bovine and human serum albumins revealed that they exhibit higher affinities for Mn(II) than OVA, most likely due to their essentially different physiological roles. These findings suggest that OVA does not play a role in the transport and storage of manganese; however, it may be involved in embryo protection from manganese-induced toxicity.

Keywords: EPR spectroscopy; manganese; metal binding; ovalbumin



Citation: Vesković, A.; Bondžić, A.M.; Popović Bijelić, A. The Role of Ovalbumin in Manganese Homeostasis during Chick Embryogenesis: An EPR Spectroscopic Study. *Molecules* **2024**, *29*, 3221. <https://doi.org/10.3390/molecules29133221>

Academic Editors: Feng Wang and Andrew Clayton

Received: 6 June 2024

Revised: 1 July 2024

Accepted: 5 July 2024

Published: 7 July 2024



Copyright: © 2024 by the authors. Licensee MDPI, Basel, Switzerland. This article is an open access article distributed under the terms and conditions of the Creative Commons Attribution (CC BY) license (<https://creativecommons.org/licenses/by/4.0/>).

1. Introduction

Ovalbumin (OVA) constitutes over 50% of total hen-egg-white proteins, making it the predominant protein in the albumen. Additionally, OVA has been identified in other components of the egg, including the yolk, the vitelline membrane, and the eggshell [1]. Despite not exhibiting inhibitory activity towards serine and cysteine proteases, this globular glycoprotein of ~45 kDa has been classified within the serpin superfamily [1,2]. OVA is composed of 385 amino acids, including six cysteines, of which only two form a single disulfide bond. The determined crystal structure has revealed that almost all of the polypeptide chain forms a defined secondary structure, a mixture of α -helices and β -sheets [3,4]. OVA has been shown to be heterogeneous, both with respect to its covalently linked carbohydrate chain [5,6] and to the extent of phosphorylation of the two serine side chains [7]. Moreover, native OVA is mostly found in its dephosphorylated form [8]. In addition to its antioxidant properties due to the presence of free sulfhydryl groups, OVA also exhibits anticancer, antihypertensive, antimicrobial, and immune-modulating activities [2,9]. These properties have been recognized as advantageous for its various biomedical applications. Due to its well-documented immunogenic efficacy, it has been extensively utilized as a model protein antigen in vaccine development [10]. OVA-based nanoparticles have been shown as effective carriers for epigallocatechin-3-gallate in the treatment of ulcerative colitis [11]. OVA-coated Fe₃O₄ nanoparticles have exhibited promising results as reservoirs for chlorogenic acid, enhancing its anticancer effectiveness in vitro [12]. Recently, the Zn(II)/ZnO-OVO hybrid nanocomplex has demonstrated excellent antibacterial and

antifungal activity, with the potential for application in antimicrobial formulations [13]. Certainly, these findings reveal that metal complexes/conjugates of OVA may find significant applications in biosensing, drug delivery, and diagnostics. In this context, a new type of fluorescent OVA-modified Au nanocluster (OVA-AuNC) sensor has been developed for the detection of ascorbic acid [14]. In another study, fluorescent OVA-AuNCs were shown to detect salicylaldehyde [15]; moreover, the salicylaldehyde/OVA-AuNCs nano-assembly was found to be a highly selective and sensitive probe for the detection of Hg^{2+} and folic acid [15]. Finally, it should be mentioned that OVA has also found extensive uses in the production of functional foods and pharmaceuticals due to its unique foaming, gelling, and emulsifying characteristics [16,17].

Despite being the first protein isolated in pure form from egg white, its actual physiological function is not fully elucidated. Found in its dephosphorylated form in egg yolk, OVA is proposed to mainly serve as a source of amino acids, supporting embryo growth and development [4]. A recent study has investigated if OVA, like serum albumins, may participate in fatty acid (FA) transport; however, it was concluded that OVA lacks a specific FA binding site [18,19]. The potential role of OVA in the transport and storage of metal ions has also been assessed [20]. A polarographic study has indicated the binding of Cu^{2+} and Cd^{2+} to the carboxyl and imidazole groups of the protein [21]. A single strong affinity binding site for various divalent and trivalent cations, including Mn^{2+} , Co^{2+} , Cu^{2+} , Zn^{2+} , Gd^{3+} , and Dy^{3+} , was detected by magnetic resonance water proton relaxation rate enhancements. Additionally, the presence of secondary, low-affinity binding sites was suggested [22].

In vivo, OVA presumably has a vital role in embryo nutrition, hydration, and antimicrobial protection. It has been shown that OVA migrates into the yolk and, subsequently, through the yolk sac membrane into the embryo [23]. Namely, starting from the 11th day of incubation, the egg-white proteins enter the amniotic fluid to be orally absorbed by the embryo [1,23]. The yolk contains essential minerals for the developing embryo, including manganese, iron, zinc, copper, calcium, and phosphorous [24]. The reported average contents of minerals (in mg per 100 g) of raw egg yolk and egg white, respectively, are as follows: Mn (0.055 and 0.011), Fe (2.73 and 0.08), Zn (2.30 and 0.03), Cu (0.077 and 0.023), Ca (129 and 7), and P (390 and 15) [25]. Manganese, as a cofactor for key metabolic and antioxidant enzymes, is vital for growth and development; its deficiency in humans and animals can lead to seizures, growth retardation, skeletal defects, diminished reproductive function, abnormal glucose tolerance, and altered metabolism [26,27]. It has also been found that manganese, besides calcium and vitamin D, is involved in maintaining optimal eggshell quality by promoting mucopolysaccharide synthesis. In this regard, studies have shown that supplemental manganese enhances thickness and fracture resistance, thus reducing damaged eggs [28]. To minimize economic losses, various strategies are currently implemented to enhance egg quality, with a primary focus on improving eggshell physical properties [29,30]. Namely, manganese is added to the hen diet, whether as sulfate or in inorganic form; however, excessive manganese exposure can cause neurotoxicity, leading to a Parkinson's disease-like condition called manganism [26]. The normal mitochondrial function may be disrupted by manganese overload through mitochondrial ROS increase, inhibition of ATP production, and membrane permeability alteration, further causing mitochondrial dysfunction and eventually metabolic syndrome or other metabolic diseases [27]. Therefore, it is important to elucidate if OVA may be involved in the regulation of manganese levels in the egg, since this protein has been identified in multiple embryo organs and proposed to constitute a dynamic participant in organ cell development [23]. Moreover, as exposure to manganese in humans primarily occurs through food consumption in addition to skin absorption [31], it is imperative to know if a manganese-supplemented hen diet may possibly lead to high manganese content in eggs, particularly bound to OVA.

In this study, the binding of Mn(II) to OVA was investigated using X-band EPR spectroscopy. In addition, a specific graphical representation of the results is proposed, from which it is possible to obtain the total number of Mn(II) binding sites on any protein and distinguish between strong and weak binding sites. UV/vis and fluorescence spectro-

scopies were used to inspect possible changes in the OVA tertiary structure upon Mn(II) binding. Subsequently, Mn(II) binding was investigated for two other proteins, bovine serum albumin (BSA) and human serum albumin (HSA), and compared to OVA. These proteins were chosen due to their ability to bind and transport hundreds of endogenous and exogenous compounds, including metal cations. The aim of this study was to gain a better understanding of OVA's role in the storage and regulation of manganese levels in vivo.

2. Results and Discussion

2.1. EPR Spectroscopy

2.1.1. The Binding of Mn(II) to OVA

EPR spectroscopy can be used to investigate systems with unpaired electrons, such as free radicals and paramagnetic metals. Due to their extremely short spin–lattice (T_1) relaxation times, EPR spectroscopy of metals is usually performed below 77 K since above this temperature the signals are broadened beyond detection. Namely, the lowering of the temperature slows down the spin–lattice relaxation, which increases the lifetime of the molecule in the excited state and, consequently, reduces the homogenous line-width (according to the Heisenberg's uncertainty relation, the line-width is inversely proportional to the lifetime of the excited state) [32]. The low-temperature EPR spectroscopy provides essential information on the binding of metal ions to proteins and other biomolecules, such as their oxidation state, coordination environment and symmetry, and stoichiometry. Manganoproteins have been extensively studied by low-temperature EPR spectroscopy with the aim to characterize their active sites [33]. Since the samples for low-temperature EPR measurements are frozen, it is even possible to gain insight into the structure of short-lived intermediates containing Mn(III) or Mn(IV) oxidation states formed during protein–substrate catalytic reactions. Nevertheless, EPR spectroscopic studies of Mn(II) are also possible at room temperature due to the relatively long T_1 relaxation time of Mn(II) compared to other metals [34]. Mn(II) shows an isotropic EPR sextet, i.e., the signal is split into six equal lines due to the hyperfine coupling of the unpaired electrons with the ^{55}Mn nuclear spin ($I = 5/2$) [35]; however, this signal can arise only from the uncoordinated, free Mn(II) in solution—specifically the divalent hexaquo–manganous complex $[\text{Mn}(\text{H}_2\text{O})_6]^{2+}$ —and not from the protein-bound cation that can be seen by low-temperature EPR spectroscopy [36–39]. Namely, it has been suggested that upon Mn(II) binding to proteins, the rotational freedom of Mn(II) becomes restricted due to the tumbling rate of the protein molecule, which is responsible for the apparent disappearance of the room-temperature EPR signal. In this respect, room-temperature EPR represents a highly sensitive spectroscopic technique for the study of manganese binding to proteins as it provides a quantitative assessment of the unbound Mn(II), from which the concentration of the protein-bound Mn(II) can be deduced.

Figure 1 (black line) shows the room-temperature EPR spectrum of 0.5 mM OVA incubated with 1 mM MnCl_2 . This signal arises from the free Mn(II) in water ($[\text{Mn}(\text{H}_2\text{O})_6]^{2+}$) since the protein-bound Mn(II) does not exhibit a room-temperature EPR signal [36–39]. Upon OVA denaturation by 1 mM perchloric acid, the protein-bound manganese is liberated, and the EPR signal is accordingly increased (Figure 1, blue line). Again, this signal arises only from the unbound Mn(II). To quantitate the amount of free Mn(II) in both cases, the normalized intensity (the peak-to-peak amplitude) of the first line in the EPR spectra was measured (marked with I_{bd} and I_{ad} in Figure 1), and the concentration of Mn(II) was determined from the calibration plot for MnCl_2 in deionized water (Figure S1 in Supplementary Materials). It should be pointed out that the quantitation of an EPR-active species using a calibration plot is possible here since the different signals have the same line-widths and line-shapes, and were measured under the same experimental conditions. The concentration of Mn(II) in the black spectrum was found to be 0.5 mM, and the concentration of Mn(II) in the blue spectrum was 1 mM. The first corresponds to the unbound Mn(II) concentration, $[\text{Mn}_{\text{ub}}]$, while the latter corresponds to the total concentration of

Mn(II) initially added to OVA [Mn_{tot}]; therefore, the concentration of the protein-bound Mn(II), [Mn_b], can be obtained as the difference of the two, [Mn_b] = [Mn_{tot}] – [Mn_{ub}], here equal to 0.5 mM.

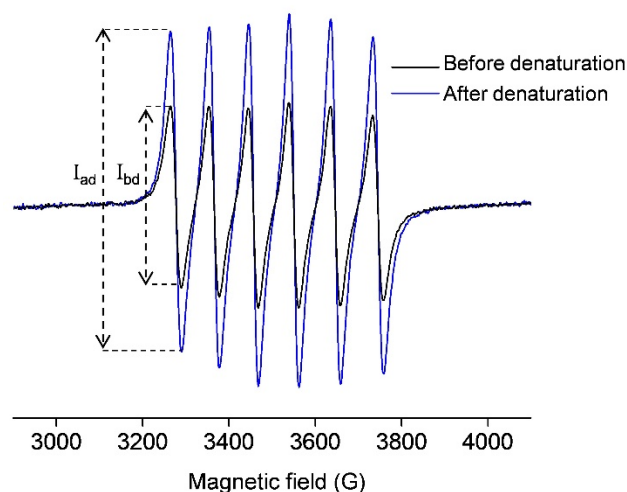


Figure 1. Room-temperature X-band EPR spectra of 0.5 mM OVA (in deionized water, pH 5.5) incubated with 1 mM $MnCl_2$, before (black) and after (blue) denaturation with 1 mM perchloric acid (pH 3). The signals arise only from free Mn(II) in water ($[Mn(H_2O)_6]^{2+}$). The intensities of the first lines in both spectra, from which the concentrations of Mn(II) were determined, are marked with I_{bd} and I_{ad} (before and after denaturation, respectively).

In order to confirm the presence of the OVA-bound Mn(II) in the non-denatured sample containing 0.5 mM OVA and 1 mM $MnCl_2$, the EPR spectrum was measured at 77 K (Figure 2a). This six-line signal, centered at $g = 2$, displays five higher-field hyperfine (forbidden) transitions caused by second-order effects due to cross products of the electron and nuclear spin operators and is characteristic of protein-bound Mn(II) ions [35,40,41]. Moreover, the spectrum shown in Figure 2a also contains a background signal (approximated with the dashed line), which arises from the unbound Mn(II) in water. Specifically, as observed from Figure 2b, free Mn(II) in water exhibits a very broad low-intensity signal at 77 K. The slope of this signal is increased with increasing Mn(II) concentrations, confirming it arises from a paramagnetic species. In general, the intensity and hyperfine couplings in Mn(II) EPR spectra are extremely sensitive to the nature of the ligands, and depend on the strength and geometry of the metal–ligand coordination bonds [35,42]; therefore, the shape and intensity of the signal shown in Figure 2b is the result of the very weak coordination of Mn(II) by water molecules in the $[Mn(H_2O)_6]^{2+}$ complex.

Finally, it should be pointed out that, in principle, the amount of the protein-bound Mn(II) could be determined by double integration of the EPR signal measured at 77 K [43], shown in Figure 2a; however, this would require prior signal deconvolution and baseline correction. Also, the calibration plot could not be obtained for $MnCl_2$ but rather a standard solution of 1 mM $CuSO_4$ in 50 mM EDTA would need to be used [34,44]. Therefore, it seems reasonable that for the purpose of this study, the methodology for the determination of Mn(II) binding to OVA should involve the use of room-temperature EPR spectroscopy, rather than “the more demanding” low-temperature EPR.

However, the low-temperature EPR spectrum shown in Figure 2a contains valuable information regarding the structural environment of the Mn(II) binding site on OVA, which can be obtained by measuring the hyperfine coupling constants A_{hfc} (i.e., the distances between hyperfine peaks in the spectrum). The spectrum exhibits an A_{hfc} -strain (distribution in A_{hfc} values), which is most likely caused by the existence of slightly different protein conformations in the sample [34]. The determined average value of A_{hfc} was 96 G (260 MHz), suggesting that Mn(II) is octahedrally coordinated to oxygen ligands [35].

Indeed, it has been suggested that the carboxylate side chains from aspartate and glutamate near the N-terminal of OVA may act as Mn(II) ligands [22]. The same study has proposed that the primary ligand for Mn(II) has a $pK_a > 8$, pointing to tyrosine and lysine side chains.

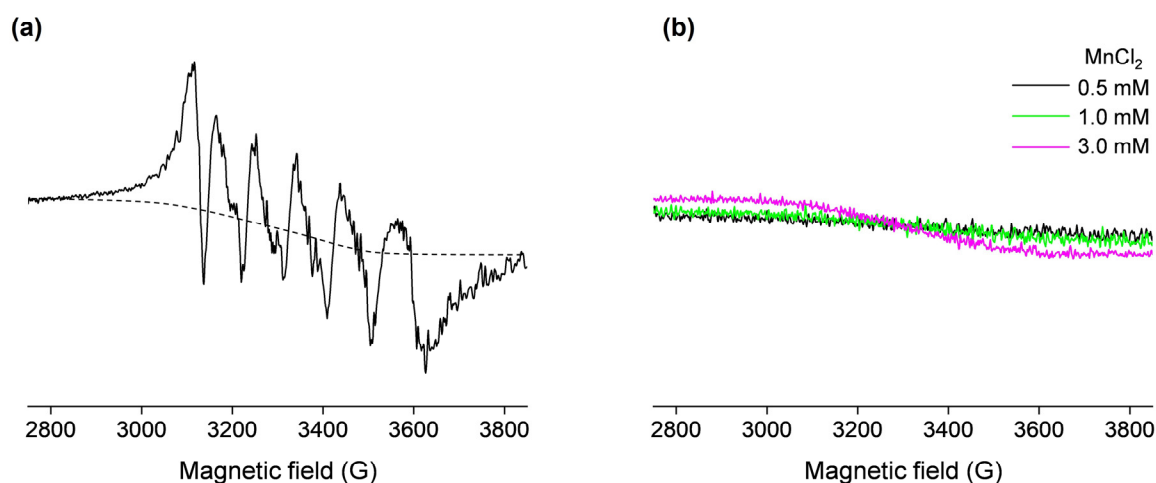


Figure 2. The 77 K X-band EPR spectra of (a) 0.5 mM OVA (in deionized water, pH 5.5) incubated with 1 mM $MnCl_2$ (the dashed line shows the approximated background signal that arises from the unbound Mn(II)); (b) 0.5, 1, and 3 mM $MnCl_2$ in deionized water (black, green, and magenta lines, respectively). The spectra in (a) and (b) are shown on the same scale.

2.1.2. The Determination of the Total Number of Mn(II) Binding Sites on OVA

Mn(II) binding to OVA was investigated for the metal:protein ratios in the range of 0.2–10, maintaining the concentration of OVA constant (0.5 mM). The concentrations of unbound Mn(II), $[Mn_{ub}]$, were determined from the intensities of the first line in the room-temperature EPR spectra (Figure S2 in Supplementary Materials), as described above. The protein-bound Mn(II) concentrations, $[Mn_b]$, were obtained from $[Mn_b] = [Mn_{tot}] - [Mn_{ub}]$. Next, the molar fractions of the unbound and bound Mn(II) ($[Mn_{ub}]/[Mn_{tot}]$ and $[Mn_b]/[Mn_{tot}]$) were plotted as the function of the total Mn(II):protein ratio, $[Mn_{tot}]/[OVA]$, Figure 3a. Note that the data points are simply connected by dashed lines only for clarity of observation and not fitted with a specific function. It is observed that at $[Mn_{tot}]/[OVA]$ ratios < 2 , the amount of $[Mn_b]$ is greater than $[Mn_{ub}]$, and at $[Mn_{tot}]/[OVA]$ ratios > 2 , the amount of $[Mn_b]$ is smaller than $[Mn_{ub}]$. For $[Mn_{tot}]/[OVA] = 2$, the dashed lines intersect, and $[Mn_{ub}] = [Mn_b]$. This shows that for $[Mn_{tot}] = 1$ mM, $[Mn_{ub}] = [Mn_b] = 0.5$ mM, confirming the result obtained from the protein-denaturation experiment (Figure 1).

In order to determine the total number of Mn(II) binding sites on OVA, the unbound and bound Mn(II):protein ratios ($[Mn_{ub}]/[OVA]$ and $[Mn_b]/[OVA]$) were plotted vs. the total Mn(II):protein ratio, $[Mn_{tot}]/[OVA]$, Figure 3b. Note that $[Mn_b]/[OVA]$ represents the fraction of the protein with bound Mn(II); therefore, it defines the number of bound Mn(II) per one molecule of OVA. From the plot in Figure 3b, it is observed that the amount of $[Mn_b]/[OVA]$ (black squares) is almost linearly increased up to $[Mn_{tot}]/[OVA] = 2$. For $[Mn_{tot}]/[OVA] > 2$, a saturation of $[Mn_b]/[OVA]$ occurs, and finally, a plateau is reached at $[Mn_{tot}]/[OVA] = 5$ and maintained up to $[Mn_{tot}]/[OVA] = 10$. This implies that there are at least two types of Mn(II) binding. The first occurs up to $y = 1$ ($[Mn_{ub}]/[OVA] = [Mn_b]/[OVA] = 1$) (Figure 3b, yellow region), where the protein-bound Mn(II) concentration linearly increases and exceeds the concentration of the unbound Mn(II). The second occurs up to $y = 2$ (Figure 3b, blue region), where the unbound Mn(II) starts to dominate, while the protein-bound Mn(II) concentration starts to saturate and finally reaches a plateau for $[Mn_{tot}]/[OVA] = 5$. These two regions are likely to correspond to stronger and weaker Mn(II) binding to OVA, respectively, as will be discussed further.

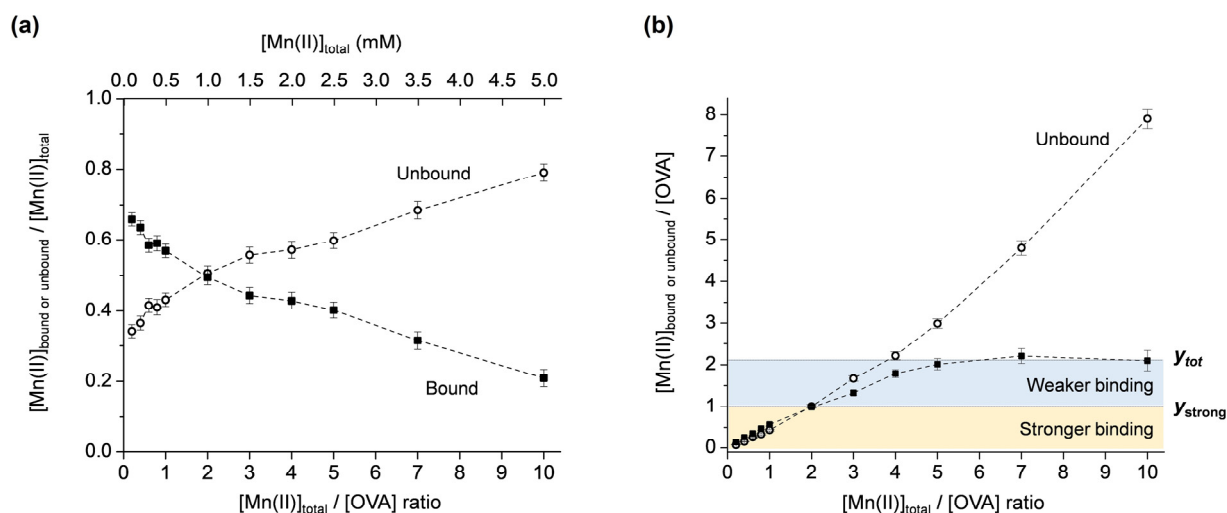


Figure 3. (a) Molar fractions of the unbound and bound Mn(II) ($[Mn_{ub}]/[Mn_{tot}]$ and $[Mn_b]/[Mn_{tot}]$) vs. $[Mn_{tot}]/[OVA]$ ratio. (b) Unbound and bound Mn(II):protein ratios ($[Mn_{ub}]/[OVA]$ and $[Mn_b]/[OVA]$) vs. $[Mn_{tot}]/[OVA]$ ratio. The yellow and blue regions correspond to stronger and weaker Mn(II) binding to OVA; y_{tot} and y_{strong} denote the total number and the number of strong Mn(II) binding sites to OVA, respectively.

The graphical representation of the results in Figure 3b allows for a straightforward determination of the total number of Mn(II) binding sites on OVA, directly from the y -axis value that corresponds to the $[Mn_b]/[OVA]$ curve plateau, here abbreviated as y_{tot} . The number of strong binding sites can be determined from the y -axis value that corresponds to the point of intersection of the $[Mn_b]/[OVA]$ and $[Mn_{ub}]/[OVA]$ curves, here abbreviated as y_{strong} . Namely, as discussed above for Figure 3a, at the curve intersection point, the molar fractions of the bound and unbound Mn(II) are equal ($=0.5$). Before this point $[Mn_b]/[Mn_{tot}] > [Mn_{ub}]/[Mn_{tot}]$, and after this point $[Mn_b]/[Mn_{tot}] < [Mn_{ub}]/[Mn_{tot}]$. This suggests that OVA displays two different affinities for Mn(II) binding before and after the point of intersection. The higher affinity is displayed up to y_{strong} and the lower affinity up to y_{tot} . Therefore, it may be concluded that OVA has a total of two Mn(II) binding sites ($y_{tot} = 2$), of which one is a stronger binding site ($y_{strong} = 1$). Moreover, OVA binds a maximum of two Mn(II) ions per protein molecule, even in a 10-fold excess of the metal. These results are in relatively good agreement with the NMR relaxometric study that has shown that native OVA possesses one strong binding site for Mn(II) ($K_d \approx 6 \times 10^{-4}$ M); the alkaline phosphatase-treated OVA has one site with slightly weaker affinity ($K_d \approx 8.3 \times 10^{-4}$ M); while the acid phosphatase-treated OVA has two equivalent sites with much weaker affinities ($K_d \approx 1.3 \times 10^{-3}$ M) [22]. It should be highlighted here that currently there are no other data in the literature reporting on Mn(II)/OVA interactions. The dissociation constants determined in this work for the two non-equivalent binding sites [45] on OVA are $K_{d1} = (5.0 \pm 0.7) \times 10^{-4}$ M and $K_{d2} = (8.0 \pm 1.1) \times 10^{-4}$ M, implying a slightly weaker binding of the second Mn(II) ion to OVA.

Typically, the total number of protein-binding sites for a specific ligand is determined from the x -axis intercept of the least-squares data fits in the Scatchard plot [46]. Scatchard analysis can also indicate if the protein contains sites with different affinities towards the ligand. However, it does not provide the exact number of stronger and weaker binding sites, which can be obtained from the plot ($[Mn_{ub}]/[OVA]$ and $[Mn_b]/[OVA]$) vs. $[Mn_{tot}]/[OVA]$, Figure 3b) proposed in this study.

2.1.3. The Binding of Mn(II) to BSA and HSA

The described methodology was applied for the investigation of Mn(II) binding to two mammalian serum albumins, BSA and HSA. Both albumins were chosen since there is emerging evidence that although they exhibit high sequence similarity, their binding

abilities are different [47,48]. As performed for OVA, the molar fractions of the unbound and bound Mn(II) were first plotted vs. the total Mn(II):protein ratio (Figure 4a for BSA and Figure 4c for HSA). It should be noted that the plot for HSA also contains data points (shown in red) that were taken from reference [49] for the defatted protein at pH 7, showing good agreement at low Mn(II):protein ratios. Subsequently, the second plot showing the unbound and bound Mn(II):protein ratios vs. the total Mn(II):protein ratio was constructed for both albumins (Figure 4b for BSA and Figure 4d for HSA). As proposed, the specific graphical representation of the results allows for the determination of the total number of binding sites on the protein, as well as the number of strong binding sites. The results indicate that, in the investigated Mn(II)-concentration range, BSA has a total of ~ 4 Mn(II) binding sites, of which two are stronger ($y_{\text{tot}} = 3.85$ and $y_{\text{strong}} = 2$, Figure 4b), and that HSA has a total of ~ 3 Mn(II) binding sites, of which one is stronger ($y_{\text{tot}} = 2.80$ and $y_{\text{strong}} = 1$, Figure 4d).

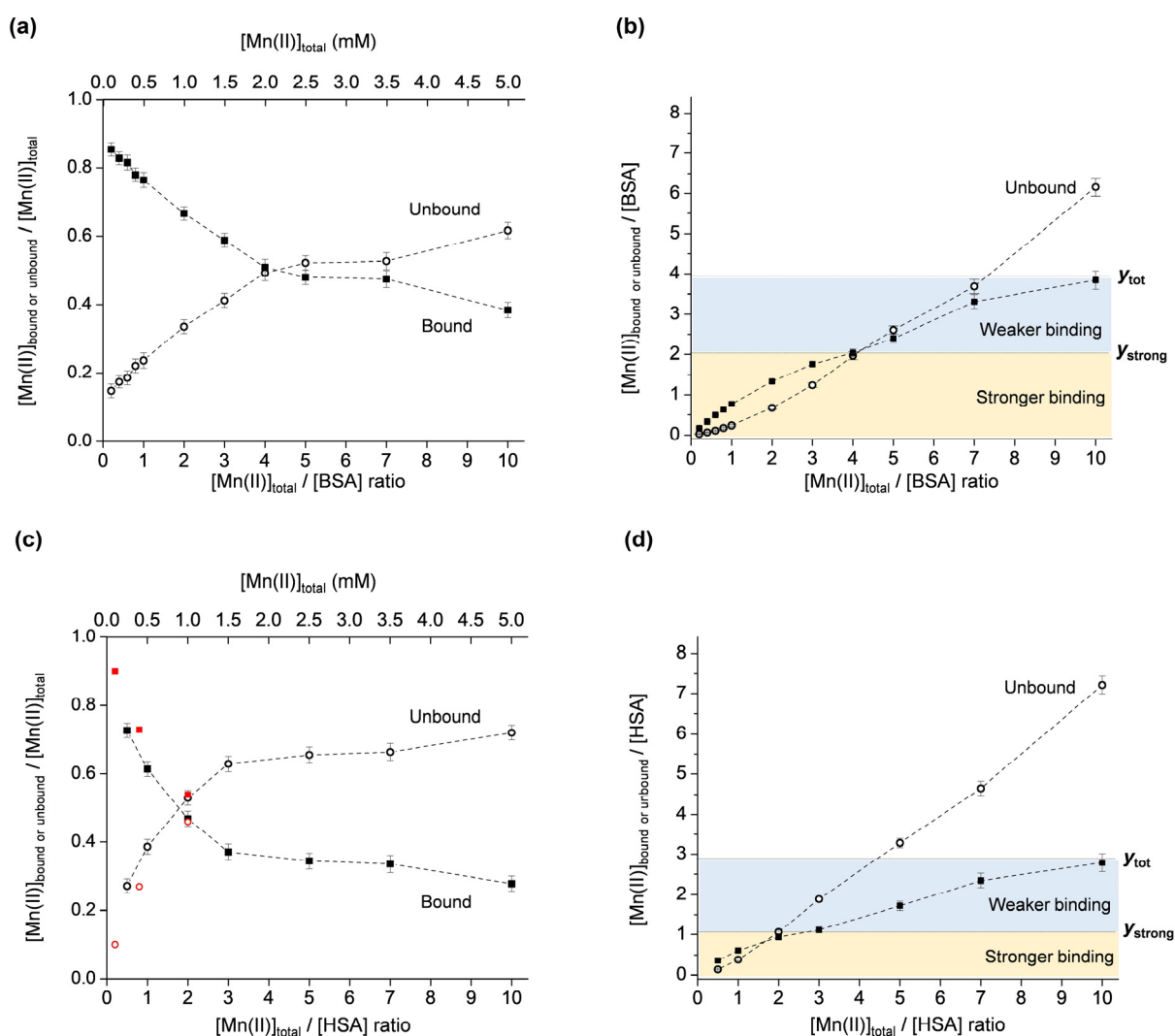


Figure 4. Molar fractions of the unbound and bound Mn(II) ($[\text{Mn}_{\text{ub}}]/[\text{Mn}_{\text{tot}}]$ and $[\text{Mn}_{\text{b}}]/[\text{Mn}_{\text{tot}}]$) vs. $[\text{Mn}_{\text{tot}}]/[\text{protein}]$ ratio, for BSA (a) and HSA (c). Unbound and bound Mn(II)-protein ratios ($[\text{Mn}_{\text{ub}}]/[\text{protein}]$ and $[\text{Mn}_{\text{b}}]/[\text{protein}]$) vs. $[\text{Mn}_{\text{tot}}]/[\text{protein}]$ ratio, for BSA (b) and HSA (d). The yellow and blue regions correspond to stronger and weaker Mn(II) binding to BSA or HSA, and y_{tot} and y_{strong} denote the total number, and the number of strong Mn(II) binding sites on BSA or HSA, respectively. The plot in (c) also shows data points in red taken from [49] obtained by ^1H NMR relaxometry.

It is evident that in the investigated Mn(II):protein = 0.2–10 ratio range, Mn(II) binding to OVA is different than to HSA and BSA. OVA exhibits binding site saturation (observed as the plateau at $y = 2$ for ratios $[\text{Mn}_{\text{tot}}]/[\text{OVA}] = 5\text{--}10$, in Figure 3b), while BSA and HSA do not display a plateau (Figures 4b and 4d, respectively). It is, however, expected that the binding site saturation for BSA and HSA would occur for higher $[\text{Mn}_{\text{tot}}]/[\text{SA}]$ ratios, specifically greater than 10. The different binding modes of OVA and BSA/HSA are likely determined by their structures and physiological functions. The fact that even in a 10-fold excess of Mn(II), OVA does not bind more than two Mn(II) ions, may suggest that it does not play a role in the transport and storage of manganese. However, it may be involved in maintaining manganese homeostasis during early embryo development by preventing excessive Mn(II) concentrations in the albumen, and, subsequently, in the amniotic fluid and embryo. On the other hand, BSA and HSA are carrier proteins, transporting various substances such as fatty acids, bilirubin, hormones (e.g., thyroxine, cortisol), drugs, as well as metal ions or complexes through the bloodstream. Although albumins are not primary transporters of manganese, the interaction of manganese with BSA and HSA has been confirmed, primarily by NMR relaxometry. The available literature data are not in complete agreement (most probably due to different protein purities, pH, ionic strengths, temperatures, and sample incubation times), and here it is summarized chronologically for both proteins. In earlier studies, it was reported that BSA contains one strong ($K_d \approx 3.7 \times 10^{-5}$ M) and five weak ($K_d \approx 3 \times 10^{-4}$ M) binding sites [50], and that HSA contains two equivalent sites ($K_d \approx 6 \times 10^{-5}$ M, or $K_d \approx 1.3 \times 10^{-4}$ M for the defatted protein) for the binding of Mn(II) [51]. In another study using equilibrium dialysis, it was proposed that both HSA and BSA have approximately two strong binding sites for Mn(II), specifically, 1.8 sites for HSA ($K_{d1} \approx 8.3 \times 10^{-5}$ M, $K_{d2} \approx 1.4 \times 10^{-4}$ M), and 1.9 sites for BSA ($K_{d1} \approx 6.7 \times 10^{-5}$ M, $K_{d2} \approx 1.3 \times 10^{-4}$ M) [52]. Later, it was shown that HSA possesses one strong ($K_d \approx 1.3 \times 10^{-4}$ M) binding site for Mn(II) ions per protein molecule, and several weaker binding sites [53]. These findings were based on the analysis of ^1H T_1 as the function of magnetic field strength, and of ^{17}O T_2 as the function of temperature, allowing the determination of various parameters involved in the relaxation process of the paramagnetic Mn(II)–HSA adduct. Furthermore, ^1H NMR relaxometry has shown that Mn(II) binds to two independent sites on HSA ($K_{d1} \approx 1.1 \times 10^{-4}$ M and $K_{d2} \approx 1.2 \times 10^{-3}$ M), and that the primary binding site for Mn(II) corresponds to the secondary binding site for Zn(II), while the secondary binding site for Mn(II) corresponds to the primary binding site for Zn(II), specifically, the multimetal binding site A [49]. The binding of Mn(II) to the multimetal binding site A on HSA, with two inner-sphere water ligands that undergo rapid exchange, has later been confirmed by ^{17}O NMR [54]. More recently, the interaction of Mn(II)/Mn(III) with BSA, investigated using fluorescence, UV/vis, and FTIR spectroscopies, has suggested moderate binding ($K_d \approx 1.4 \times 10^{-3}$ M) of one manganese ion to the protein [31]. Finally, the results from this study, using EPR spectroscopy, show that HSA has one stronger ($K_d = (1.8 \pm 0.4) \times 10^{-4}$ M) and two weaker ($K_d = (2.6 \pm 0.9) \times 10^{-3}$ M) Mn(II) binding sites, and BSA has two stronger ($K_d = (1.9 \pm 0.2) \times 10^{-4}$ M) and two weaker ($K_d = (4.7 \pm 1.5) \times 10^{-3}$ M) Mn(II) binding sites, determined for globulin-free, fatty acid-free 0.5 mM protein preparations in deionized water (pH 5.5) in the 0.1–5 mM Mn(II) concentration range.

2.2. Fluorescence and UV/vis Absorption Spectra of OVA in Presence of Mn(II)

The binding of Mn(II) to OVA was additionally investigated by fluorescence and UV/vis absorption spectroscopies. The intrinsic fluorescence of OVA is due to the presence of three tryptophan and ten tyrosine residues [3,4]. Fluorescence spectroscopy has been successfully used to investigate the interaction of OVA with various compounds, such as L-ascorbic acid, α -tocopherol, procyanidin B3, β -carotene, and astaxanthin [55], resveratrol [56], folic acid [57], Monascus pigment [58], caffeic acid [59], as well as metal-containing nanoparticles with gold and silver [60] or iron oxide [61]. The fluorescence emission spectra of OVA, excited at 280 nm, in the absence and presence of Mn(II) at protein:metal ratios of

1:1, 1:2, 1:5, and 1:10 are shown in Figure 5a. No fluorescence quenching is observed up to the 1:2 ratio, and insignificant quenching (ca. 5%) occurs for the 1:10 ratio. Moreover, there were no observable shifts in the spectra towards lower or higher wavelengths. This indicates that either the binding of Mn(II) to OVA does not induce protein conformational changes, which would in principle affect the local amino acid environment surrounding the fluorophores, or that the OVA binding sites for Mn(II) are not located in close proximity of the fluorophores.

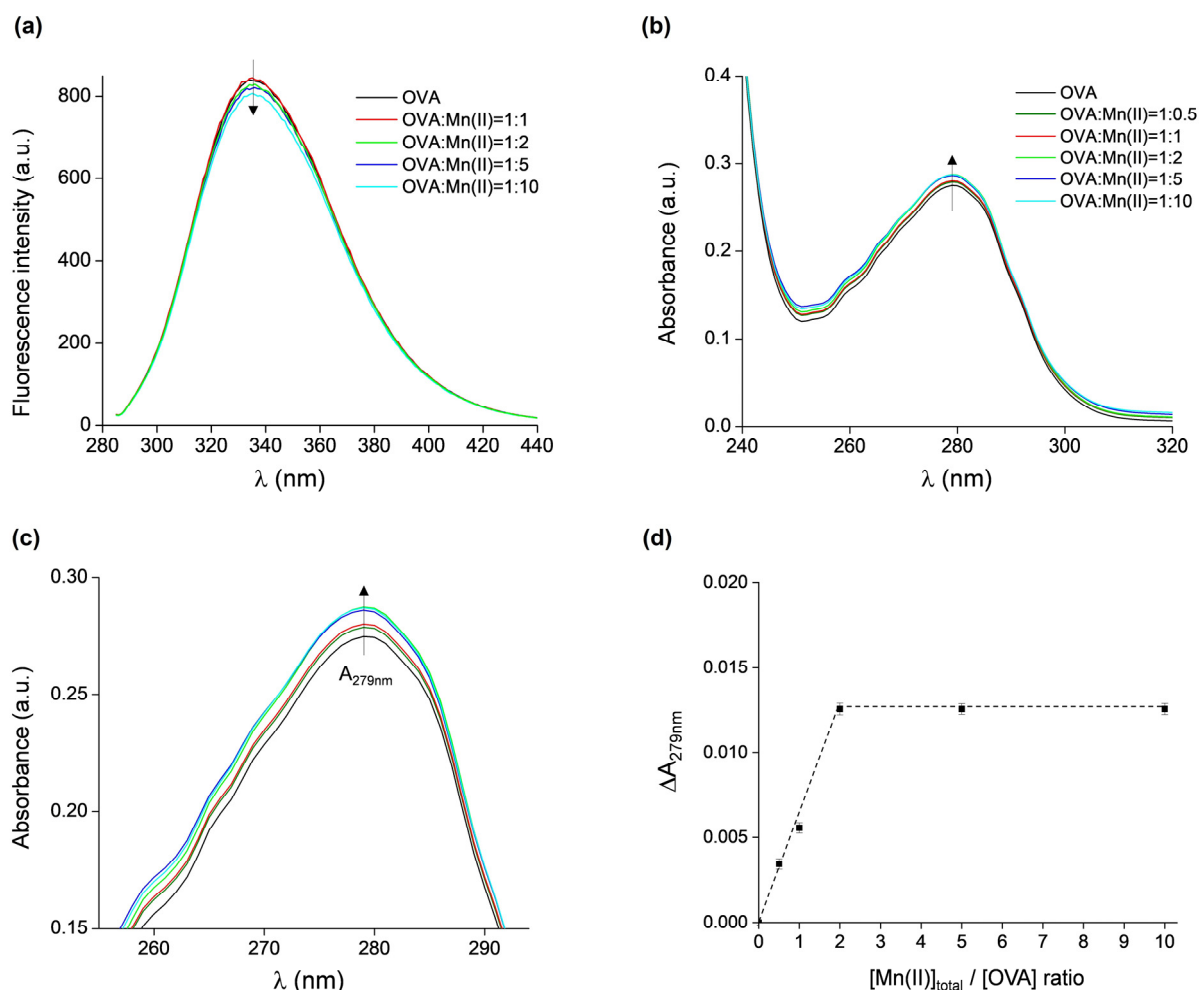


Figure 5. (a) Fluorescence emission spectra of OVA, excited at 280 nm, in the presence of increasing concentrations of Mn(II). (b) UV/vis absorption spectra of OVA in the presence of increasing concentrations of Mn(II). (c) Magnified part of UV/vis spectra shown in (b) (with the same color scheme as in (b)). (d) The difference in absorbance measured at 279 nm of OVA alone and of samples containing OVA in presence of Mn(II) vs. $[\text{Mn}_{\text{tot}}]/[\text{OVA}]$ ratios, $\Delta A_{279\text{nm}} = A_{279\text{nm}}(\text{OVA} + n\text{Mn}) - A_{279\text{nm}}(\text{OVA})$, $n = 0, 0.5, 1, 2, 5, 10$.

The UV/vis spectra of the same samples (and additionally the protein:metal ratio of 1:0.5) showed only a minor increase in absorbance when measured at 279 nm ($A_{279\text{nm}}$) with increasing Mn(II) concentrations (Figure 5b), confirming that the binding of Mn(II) does not affect the tertiary structure of OVA. However, the differences in $A_{279\text{nm}}$ of OVA alone and of the OVA + Mn(II) samples are measurable (for clarity, a magnified part of Figure 5b is given in Figure 5c), and they were plotted as the function of $[\text{Mn}_{\text{tot}}]:[\text{OVA}]$ ratio (Figure 5d). It is observed that $\Delta A_{279\text{nm}}$ increased up to $[\text{Mn(II)}]_{\text{tot}}:[\text{OVA}] = 2$, after which a plateau is reached. This result shows that a maximum of two Mn(II) ions can bind per one molecule of OVA, corroborating the findings from the EPR measurements.

3. Materials and Methods

3.1. Chemicals

Ovalbumin (OVA, purity $\geq 98\%$), bovine serum albumin (BSA, protease-free, fatty acid-free, globulin-free, purity $\geq 98\%$), human serum albumin (HSA, fatty acid-free, globulin-free, purity $\geq 99\%$), $\text{MnCl}_2 \cdot 4\text{H}_2\text{O}$, and perchloric acid were purchased from Sigma-Aldrich, St. Louis, MO, USA. All samples were prepared using deionized water (Milli-Q, 18 M Ω -cm, Merck KGaA, Darmstadt, Germany).

3.2. EPR Spectroscopy

The samples for EPR measurements contained 150 μL of 0.6 mM protein solution in deionized water, and 30 μL of the appropriate concentration of MnCl_2 to obtain metal:protein concentration ratios of 0.2, 0.4, 0.5, 0.6, 0.8, 1, 2, 3, 4, 5, 7, and 10. All samples were incubated at room temperature for 1 h. MnCl_2 solutions in deionized water in the concentration range of 0.1–6 mM were used for the Mn(II) calibration plot. A volume of 30 μL was drawn into a 1-millimeter-diameter gas-permeable Teflon tube (Zeus Industries Inc., Largo, FL, USA) and inserted into a quartz EPR cuvette (inner diameter 3 mm, Wilmad LabGlass, Vineland, NJ, USA) for spectra acquisition at room temperature. For the 77 K EPR experiments, 180 μL of samples containing Mn(II) and OVA in the metal:protein concentration ratio range of 0.2–10 were directly placed into the quartz EPR cuvette (inner diameter 3 mm, Wilmad LabGlass, Vineland, NJ, USA) and manually frozen in cold isopentane.

All experiments were performed on a Bruker Biospin Elexsys II E540 EPR spectrometer. For the 77 K measurements, the liq.N₂ dewar (WG-816-B-Q, Wilmad LabGlass, Vineland, NJ, USA) was used. The experimental parameters were as follows: For room-temperature measurements—microwave frequency 9.8 GHz, microwave power 10 mW, modulation amplitude 0.5 G, and modulation frequency 100 kHz. For 77 K measurements—microwave frequency 9.4 GHz, microwave power 1 mW, modulation amplitude 10 G, and modulation frequency 100 kHz.

3.3. Fluorescence Spectroscopy

The fluorescence emission spectra of OVA in deionized water, in the absence and presence of Mn(II) (at metal:protein ratios of 1:1, 2:1, 5:1, and 10:1), were recorded using the Agilent Cary Eclipse fluorescence spectrophotometer in the wavelength range of 285–450 nm. The excitation wavelength was 280 nm, the excitation and emission slit widths were 5 nm, and the scanning rate was 600 nm/min.

3.4. UV/vis Spectrophotometry

The absorption spectra of OVA in deionized water, in the absence and presence of Mn(II) (at metal:protein ratios of 0.5:1, 1:1, 2:1, 5:1, and 10:1), were recorded on a UV/vis spectrophotometer (Lambda 35, Perkin Elmer, Waltham, MA, USA) in the wavelength range of 240–320 nm.

3.5. Data Fitting

The dissociation constants (K_d) for Mn(II)/protein complexes were determined by fitting the data obtained from EPR measurements using a two-site binding model (Equation (1)):

$$y = B_{\max 1} \cdot x / (k_1 + x) + B_{\max 2} \cdot x / (k_2 + x), \quad (1)$$

where y is the fraction of the occupied sites on the protein; x is the free Mn(II) concentration; $B_{\max 1}$ and $B_{\max 2}$ are maximal occupancies of binding sites 1 and 2; and k_1 and k_2 correspond to the appropriate dissociation constants.

4. Conclusions

The results from this study obtained from EPR measurements show that OVA contains two binding sites with different affinities for Mn(II); moreover, it was observed that OVA

does not bind more than two Mn(II) ions per protein molecule, even in a 10-fold excess of Mn(II). This result was confirmed also by UV/vis spectroscopy. The binding of Mn(II) to OVA, or the presence of excess Mn(II), appears not to induce protein conformational changes, as evidenced by insignificant fluorescence quenching, ca. 5% for the concentration ratio OVA:Mn(II) = 1:10, and the lack of hypsochromic/bathochromic shifts. Moreover, it is likely that Mn(II) does not bind in close proximity to the fluorophores.

BSA and HSA exhibit different Mn(II) binding sites/modes compared to OVA, not displaying binding site saturation, which may be the result of their different physiological functions. It seems that OVA does not play a role in the transport and storage of manganese, however, it is likely involved in the regulation of manganese levels in vivo, possibly having a protective role from manganese overload.

The presence of the OVA-bound Mn(II) was confirmed by EPR spectroscopy at 77 K. The measured EPR hyperfine coupling constants suggest that Mn(II) is octahedrally coordinated to oxygen ligands; however, further competitive binding EPR studies at lower temperatures should be performed in order to elucidate the structural environments of the two Mn(II) binding sites on OVA.

Although low-temperature EPR spectroscopy can detect protein-bound paramagnetic metal ions and further provide information on the symmetry and nature of the ligands, it is not optimal for metal ion quantitation due to the fact that double integration is hindered by background signals. Also, the signal intensity is not a good measure since it is sensitive to the nature of the ligands. The latter is also true for room-temperature EPR spectroscopy, however, it provides here an advantage in that the highest signal intensity is observed for the uncoordinated, free Mn(II)—namely $[\text{Mn}(\text{H}_2\text{O})_6]^{2+}$ —while the protein-bound Mn(II) signal is broadened beyond detection. Therefore, the amount of the OVA-bound Mn(II) in this study was determined by measuring the amount of the unbound Mn(II) by EPR spectroscopy at room temperature.

EPR spectroscopy has not frequently been used to investigate ligand binding since it detects only species that have at least one unpaired electron; however, when the ligand is, in fact, a paramagnet like Mn(II) investigated in this study, EPR is unrivaled. Namely, fluorescence and UV/vis absorption spectroscopies provide incredibly useful information regarding the changes in the protein environment caused by ligand binding, from which it is possible to calculate the total number of binding sites; however, the quantitation of free and bound paramagnetic ligands is possible only by EPR, which ultimately allows for discriminating between the numbers of binding sites with different affinities towards the ligand.

Supplementary Materials: The following supporting information can be downloaded at <https://www.mdpi.com/article/10.3390/molecules29133221/s1>. Figure S1: The calibration plot for MnCl_2 in deionized water in the concentration range 0.1–6 mM; Figure S2: Room-temperature X-band EPR spectra of 0.5 mM OVA in deionized water, pH 5.5, incubated with MnCl_2 at different OVA:Mn(II) concentration ratios: (a) 1:0.2 (black), 1:0.4 (red), 1:0.6 (blue), 1:0.8 (green), 1:1 (purple), and (b) 1:1 (black), 1:2 (red), 1:3 (blue), 1:5 (green), 1:7 (purple), 1:10 (yellow).

Author Contributions: A.V.: conducting research—performing experiments, data collection; writing—original draft. A.M.B.: conducting research—performing experiments, data collection; writing—original draft; visualization. A.P.B.: formulation of research goals; design and development of methodology; conducting research—performing experiments; results verification; writing—original draft, review and editing; visualization; supervision; funding acquisition. All authors have read and agreed to the published version of the manuscript.

Funding: This research was supported by the Ministry of Science, Technological Development and Innovation of the Republic of Serbia (451-03-65/2024-03/200146).

Institutional Review Board Statement: Not applicable.

Informed Consent Statement: Not applicable.

Data Availability Statement: All data are contained in this article and its Supplementary Materials.

Conflicts of Interest: The authors declare that they have no known competing financial interests or personal relationships that could have appeared to influence the work reported in this paper.

References

1. Guyot, N.; Da Silva, M.; Nys, Y.; Rehault-Godbert, S. Minireview The Family Secrets of Avian Egg-Specific Ovalbumin and Its Related Proteins Y and X. *Biol. Reprod.* **2015**, *93*, 130856. [[CrossRef](#)]
2. Rostamabadi, H.; Chaudhary, V.; Chhikara, N.; Sharma, N. Food Hydrocolloids Ovalbumin, an Outstanding Food Hydrocolloid: Applications, Technofunctional Attributes, and Nutritional Facts, A Systematic Review. *Food Hydrocoll.* **2023**, *139*, 108514. [[CrossRef](#)]
3. Stein, P.E.; Leslie, A.G.W.; Finch, J.T.; Turnell, W.G.; McLaughlin, P.J.; Carrell, R.W. Crystal Structure of Ovalbumin as a Model for the Reactive Centre of Serpins. *Nature* **1990**, *347*, 99–102. [[CrossRef](#)] [[PubMed](#)]
4. Stein, P.E.; Leslie, A.G.W.; Finch, J.T.; Carrell, R.W. Crystal Structure of Uncleaved Ovalbumin at 1.95 Å Resolution. *J. Mol. Biol.* **1991**, *221*, 941–959. [[CrossRef](#)] [[PubMed](#)]
5. Atkinson, P.H.; Grey, A.; Carver, J.P.; Hakimi, J.; Ceccarini, C. Demonstration of Heterogeneity of Chick Ovalbumin Glycopeptides Using 360-MHz Proton Magnetic Resonance Spectroscopy. *Biochemistry* **1981**, *20*, 3979–3986. [[CrossRef](#)]
6. Narasimhan, S.; Harpaz, N.; Longmore, G.; Carver, J.P.; Grey, A.A.; Schachter, H. Control of Glycoprotein Synthesis. The Purification by Preparative High Voltage Paper Electrophoresis in Borate of Glycopeptides Containing High Mannose and Complex Oligosaccharide Chains Linked to Asparagine. *J. Biol. Chem.* **1980**, *255*, 4876–4884. [[CrossRef](#)] [[PubMed](#)]
7. Nisbet, A.D.; Saundry, R.H.; Moir, A.J.G.; Fothergill, L.A.; Fothergill, J.E. The Complete Amino-Acid Sequence of Hen Ovalbumin. *Eur. J. Biochem.* **1981**, *115*, 335–345. [[CrossRef](#)] [[PubMed](#)]
8. Cann, J.R. Electrophoretic Analysis of Ovalbumin. *J. Am. Chem. Soc.* **1949**, *71*, 907–909. [[CrossRef](#)]
9. Sharif, M.K.; Saleem, M.; Javed, K. Food Materials Science in Egg Powder Industry. In *Role of Materials Science in Food Bioengineering*; Grumezescu, A.M., Holban, A.M., Eds.; Academic Press: Cambridge, MA, USA, 2018; pp. 505–537. ISBN 9780128115008.
10. Ke, Y.; Li, Y.; Kapp, J.A. Ovalbumin Injected with Complete Freund's Adjuvant Stimulates Cytolytic Responses. *Eur. J. Immunol.* **1995**, *25*, 549–553. [[CrossRef](#)]
11. Gou, S.; Chen, Q.; Liu, Y.; Zeng, L.; Song, H.; Xu, Z.; Kang, Y.; Li, C.; Xiao, B. Green Fabrication of Ovalbumin Nanoparticles as Natural Polyphenol Carriers for Ulcerative Colitis Therapy. *ACS Sustain. Chem. Eng.* **2018**, *6*, 12658–12667. [[CrossRef](#)]
12. Manivel, P.; Paulpandi, M.; Chen, X. Ovalbumin-Coated Fe₃O₄ Nanoparticles as a Nanocarrier for Chlorogenic Acid to Promote the Anticancer Efficacy on MDA-MB-231 Cells. *New J. Chem.* **2022**, *46*, 12609–12622. [[CrossRef](#)]
13. Buszewski, B.; Žuvela, P.; Krol-Gorniak, A.; Railean-Plugaru, V.; Rogowska, A.; Wah Wong, M.; Yi, M.; Rodzik, A.; Sprynskyy, M.; Pomastowski, P. Applied Surface Science Interactions of Zinc Aqua Complexes with Ovalbumin at the Forefront of the Zn²⁺/ZnO-OVO Hybrid Complex Formation Mechanism. *Appl. Surf. Sci.* **2021**, *542*, 148641. [[CrossRef](#)]
14. Li, Y.; Chen, Y.; Huang, L.; Ma, L.; Chen, G. Au Nanoclusters for Sensitive Detection of Ascorbic. *Anal. Methods* **2015**, *7*, 4123–4129. [[CrossRef](#)]
15. Nakum, R.; Ghosh, A.K.; Ranjan, B.; Sahoo, S.K. Spectrochimica Acta Part A: Molecular and Biomolecular Spectroscopy Fluorescent Ovalbumin-Functionalized Gold Nanocluster as a Highly Sensitive and Selective Sensor for Relay Detection of Salicylaldehyde, Hg (II) and Folic Acid. *Spectrochim. Acta Part A Mol. Biomol. Spectrosc.* **2024**, *313*, 124143. [[CrossRef](#)]
16. Nyemb, K.; Guérin-Dubiard, C.; Dupont, D.; Jardin, J.; Rutherford, S.M.; Nau, F. The Extent of Ovalbumin In Vitro Digestion and the Nature of Generated Peptides Are Modulated by the Morphology of Protein Aggregates. *Food Chem.* **2014**, *157*, 429–438. [[CrossRef](#)] [[PubMed](#)]
17. El-Salam, M.H.A.; El-Shibiny, S. Natural Biopolymers as Nanocarriers for Bioactive Ingredients Used in Food Industries. In *Nanotechnology in the Agri-Food Industry, Encapsulations*; Grumezescu, A.M., Ed.; Academic Press: Cambridge, MA, USA, 2016; pp. 793–829. ISBN 9780128043073.
18. Vesković, A.; Nakarada, Đ.; Popović Bijelić, A. Fatty Acid Binding to Ovalbumin Studied by EPR. In Proceedings of the Regional Biophysics Conference 2022, Pécs, Hungary, 22–26 August 2022.
19. Vesković, A.; Bajuk-Bogdanović, D.; Arion, V.B.; Popović Bijelić, A. Spectroscopic Characterization of the Binding and Release of Hydrophilic, Hydrophobic and Amphiphilic Molecules from Ovalbumin Supramolecular Hydrogels. *Gels* **2023**, *9*, 14. [[CrossRef](#)] [[PubMed](#)]
20. Harischandra, D.S.; Ghaisas, S.; Zenitsky, G.; Jin, H. Manganese-Induced Neurotoxicity: New Insights Into the Triad of Protein Misfolding, Mitochondrial Impairment, and Neuroinflammation. *Front. Neurosci.* **2019**, *13*, 654. [[CrossRef](#)] [[PubMed](#)]
21. Malik, W.U.; Jindal, M.R. Polarographic Studies on the Binding of Copper(II) and Cadmium(II) with Ovalbumin. *J. Electroanal. Chem.* **1968**, *19*, 436–438. [[CrossRef](#)]
22. Goux, W.J.; Venkatasubramanian, P.N. Metal Ion Binding Properties of Hen Ovalbumin and S-Ovalbumin: Characterization of the Metal Ion Binding Site by ³¹P NMR and Water Proton Relaxation Rate Enhancements. *Biochemistry* **1986**, *25*, 84–94. [[CrossRef](#)]
23. Sugimoto, Y.; Sanuki, S.; Ohsako, S.; Higashimoto, Y.; Kondo, M.; Kurawaki, J.; Ibrahim, H.R.; Aoki, T.; Kusakabe, T.; Koga, K. Ovalbumin in Developing Chicken Eggs Migrates from Egg White to Embryonic Organs While Changing Its Conformation and Thermal Stability *. *J. Biol. Chem.* **1999**, *274*, 11030–11037. [[CrossRef](#)]
24. Uni, Z.; Yadgary, L.; Yair, R. Embryonic Development 1. *J. Appl. Poult. Res.* **2012**, *21*, 175–184. [[CrossRef](#)]

25. Réhault-Godbert, S.; Guyot, N.; Nys, Y. The Golden Egg: Nutritional Value, Bioactivities, and Emerging Benefits for Human Health. *Nutrients* **2019**, *11*, 684. [[CrossRef](#)]
26. Babadi, V.Y.; Sadeghi, L.; Shirani, K.; Malekirad, A.A.; Rezaei, M. The Toxic Effect of Manganese on the Acetylcholinesterase Activity in Rat Brains. *J. Toxicol.* **2014**, *2014*, 946372.
27. Li, L. Review Article The Essential Element Manganese, Oxidative Stress, and Metabolic Diseases: Links and Interactions. *Oxid. Med. Cell. Longev.* **2018**, *2018*, 7580707. [[CrossRef](#)] [[PubMed](#)]
28. Olgun, O. Manganese in Poultry Nutrition and Its Effect on Performance and Eggshell Quality. *World's Poult. Sci. J.* **2017**, *73*, 45–56. [[CrossRef](#)]
29. Voica, C.; Cristea, G.; Iordache, A.M.; Roba, C.; Curean, V. Elemental Profile in Chicken Egg Components and Associated Human Health Risk Assessment. *Toxics* **2023**, *11*, 900. [[CrossRef](#)]
30. Świątkiewicz, S.; Arczewska-Włosek, A.; Krawczyk, J.; Puchała, M.; Józefiak, D. Dietary Factors Improving Eggshell Quality: An Updated Review with Special Emphasis on Microelements and Feed Additives. *World's Poult. Sci. J.* **2015**, *71*, 83–94. [[CrossRef](#)]
31. Gu, J.; Yang, G.; Huang, X.; He, Q. Revealing the Complexity of Distinct Manganese Species-Protein Interactions through Multi-Spectroscopy. *Spectrochim. Acta Part A Mol. Biomol. Spectrosc.* **2021**, *260*, 119981. [[CrossRef](#)] [[PubMed](#)]
32. Weil, J.A.; Bolton, J.R. *Electron Paramagnetic Resonance: Elementary Theory and Practical Applications*, 2nd ed.; John Wiley & Sons, Inc.: Hoboken, NJ, USA, 2007; ISBN 9780471754961.
33. Wieghardt, K. The Active Sites in Manganese-Containing Metalloproteins and Inorganic Model Complexes. *Angew. Chem. Int. Ed. Engl.* **1989**, *28*, 1153–1172. [[CrossRef](#)]
34. Hagen, W.R. *Biomolecular EPR Spectroscopy*; CRC Press, Taylor & Francis Group: Boca Raton, FL, USA, 2009; ISBN 978-1-4200-5957-1.
35. Reed, G.H.; Markham, G.D. EPR of Mn(II) Complexes with Enzymes and Other Proteins. In *Biological Magnetic Resonance*; Berliner, L.J., Reuben, J., Eds.; Springer: Boston, MA, USA, 1984; pp. 73–142.
36. Cohn, M.; Townsend, J. A Study of Manganous Complexes by Paramagnetic Resonance Absorption. *Nature* **1954**, *173*, 1090–1091. [[CrossRef](#)]
37. Malmström, B.G.; Vänngård, T.; Larsson, M. An Electron-Spin-Resonance Study of the Interaction of Manganous Ions with Enolase and Its Substrate. *Biochim. Biophys. Acta* **1958**, *30*, 1–5. [[CrossRef](#)] [[PubMed](#)]
38. Reed, G.H.; Cohn, M. Electron Paramagnetic Resonance Spectra of Manganese(II)-Protein Complexes. *J. Biol. Chem.* **1970**, *245*, 662–664. [[CrossRef](#)] [[PubMed](#)]
39. Reed, G.H.; Cohn, M. Electron Paramagnetic Resonance Studies of Manganese(II)-Pyruvate Kinase-Substrate Complexes. *J. Biol. Chem.* **1973**, *248*, 6436–6442. [[CrossRef](#)] [[PubMed](#)]
40. Von Goldammer, E.; Zorn, H. Electron-Paramagnetic-Resonance Study of Manganese Ions Bound to Concanavalin A. *Eur. J. Biochem.* **1974**, *44*, 195–199. [[CrossRef](#)] [[PubMed](#)]
41. Whiting, A.K.; Boldt, Y.R.; Hendrich, M.P.; Wackett, L.P.; Que, L. Manganese(II)-Dependent Extradiol-Cleaving Catechol Dioxygenase from *Arthrobacter Globiformis* CM-2. *Biochemistry* **1996**, *35*, 160–170. [[CrossRef](#)] [[PubMed](#)]
42. Abragam, A.; Bleaney, B. *Electron Paramagnetic Resonance of Transition Ions*; Oxford University Press: London, UK, 1970.
43. Eaton, G.R.; Eaton, S.S.; Barr, D.P.; Weber, R.T. *Quantitative EPR*; Springer: Vienna, Austria, 2010; ISBN 978-3-211-92947-6.
44. Voevodskaya, N.; Lenzian, F.; Ehrenberg, A.; Gräslund, A. High Catalytic Activity Achieved with a Mixed Manganese-Iron Site in Protein R2 of Chlamydia Ribonucleotide Reductase. *FEBS Lett.* **2007**, *581*, 3351–3355. [[CrossRef](#)] [[PubMed](#)]
45. Angulo, J.; Enríquez-Navas, P.M.; Nieto, P.M. Ligand-Receptor Binding Affinities from Saturation Transfer Difference (STD) NMR Spectroscopy: The Binding Isotherm of STD Initial Growth Rates. *Chem.-Eur. J.* **2010**, *16*, 7803–7812. [[CrossRef](#)] [[PubMed](#)]
46. Voet, D.; Voet, J.G. *Biochemistry*, 4th ed.; John Wiley & Sons, Inc.: Hoboken, NJ, USA, 2010; ISBN 978-0-470-57095-1.
47. Sekula, B.; Zielinski, K.; Bujacz, A. Crystallographic Studies of the Complexes of Bovine and Equine Serum Albumin with 3,5-Diiodosalicylic Acid. *Int. J. Biol. Macromol.* **2013**, *60*, 316–324. [[CrossRef](#)] [[PubMed](#)]
48. Wang, P.-Y.; Yang, C.-T.; Chu, L.-K. Differentiating the Protein Dynamics Using Fluorescence Evolution of Tryptophan Residue(s): A Comparative Study of Bovine and Human Serum Albumins upon Temperature Jump. *Chem. Phys. Lett.* **2021**, *781*, 138998. [[CrossRef](#)]
49. Fanali, G.; Cao, Y.; Ascenzi, P.; Fasano, M. Mn(II) Binding to Human Serum Albumin: A ¹H-NMR Relaxometric Study. *J. Inorg. Biochem.* **2012**, *117*, 198–203. [[CrossRef](#)]
50. Mildvan, A.S.; Cohn, M. Magnetic Resonance Studies of the Interaction of the Manganous Ion with Bovine Serum Albumin. *Biochemistry* **1963**, *2*, 910–919. [[CrossRef](#)] [[PubMed](#)]
51. Chapman, B.E.; MacDermott, T.E.; O'Sullivan, W.J. Studies on Manganese Complexes of Human Serum Albumin. *Bioinorg. Chem.* **1973**, *3*, 27–38. [[CrossRef](#)]
52. Hong, L.; Chu-Qiao, T.; Hong-Zhi, Z.; Xing-Can, S.; Yong-Qia, Z.; Pan-Wen, S. Binding Equilibrium Study between Mn(II) and HSA or BSA. *Chin. J. Chem.* **2000**, *18*, 35–41. [[CrossRef](#)]
53. Aime, S.; Canton, S.; Geninatti Crich, S.; Terreno, E. ¹H and ¹⁷O Relaxometric Investigations of the Binding of Mn(II) Ion to Human Serum Albumin. *Magn. Reson. Chem.* **2002**, *40*, 41–48. [[CrossRef](#)]
54. Gale, E.M.; Zhu, J.; Caravan, P. Direct Measurement of the Mn(II) Hydration State in Metal Complexes and Metalloproteins through ¹⁷O NMR Line Widths. *J. Am. Chem. Soc.* **2013**, *135*, 18600–18608. [[CrossRef](#)]
55. Li, X.; Yan, Y. Comparative Study of the Interactions between Ovalbumin and Five Antioxidants by Spectroscopic Methods. *J. Fluoresc.* **2017**, *27*, 213–225. [[CrossRef](#)] [[PubMed](#)]

56. Cheng, W.; Ma, J.; Wang, S.; Lou, R.; Wu, S.; He, J.; Kang, H.; Liu, L.; Xiao, F. Interaction Mechanism between Resveratrol and Ovalbumin Based on Fluorescence Spectroscopy and Molecular Dynamic Simulation. *LWT* **2021**, *146*, 111455. [[CrossRef](#)]
57. Cen, C.; Chen, J.; Wang, W.; Zhang, J.; Yang, X.; Fu, L.; Wang, Y. Exploring the Interaction Mechanism of Dietary Protein Ovalbumin and Folic Acid: A Combination Research of Molecular Simulation Technology and Multispectroscopy. *Food Chem.* **2022**, *385*, 132536. [[CrossRef](#)]
58. Zhang, P.; Huang, X.; Fu, C.; Gong, Y.; Huang, X.; Zhang, J.; Li, X.; Song, H.; Huang, Q. Binding Mechanism of Monascus Pigment and Ovalbumin: Spectral Analysis, Molecular Docking and Molecular Dynamics Simulation. *Food Sci. Anim. Prod.* **2023**, *1*, 9240038. [[CrossRef](#)]
59. Cheng, W.; Wang, M.; Li, C.; Xiao, F.; He, J.; Liu, L.; Niu, H.; Ma, J. Study of the Weak Interaction Mechanism of Ovalbumin and Caffeic Acid Using Fluorescence Spectroscopy and Molecular Dynamics Simulation. *Spectrochim. Acta Part A Mol. Biomol. Spectrosc.* **2023**, *301*, 122966. [[CrossRef](#)]
60. Joshi, D.; Soni, R.K. Nanosecond Laser-Assisted Fabrication of Colloidal Gold and Silver Nanoparticles and Their Conjugation with S-Ovalbumin. *Plasmonics* **2018**, *13*, 1297–1308. [[CrossRef](#)]
61. Tsykhanovska, I.; Stabnikova, O.; Gubsky, S. Spectroscopic Studies of Interactions of Iron Oxide Nanoparticles with Ovalbumin Molecules. *Mater. Proc.* **2022**, *9*, 2. [[CrossRef](#)]

Disclaimer/Publisher's Note: The statements, opinions and data contained in all publications are solely those of the individual author(s) and contributor(s) and not of MDPI and/or the editor(s). MDPI and/or the editor(s) disclaim responsibility for any injury to people or property resulting from any ideas, methods, instructions or products referred to in the content.